(Received 17 December 2024, Accepted 13 February 2025, Scheduled 16 February 2025)

Ultra-Compact Photonic Isolator Based on Bias-Free Magneto-Optical Thin Films

Gianni Portela[1, 2, *], Yisheng Ni[1], Kotaro Sato[1], Yuya Shoji[1], and Hugo E. Hernandez-Figueroa[2]

[1] *Department of Electrical and Electronic Engineering, School of Engineering, Institute of Science Tokyo 2-12-1, Ookayama, Meguro-ku, Tokyo 152-8550, Japan*
[2] *School of Electrical and Computer Engineering, University of Campinas, Campinas, SP 13083-852, Brazil*

ABSTRACT: An ultra-compact isolator based on the integration of aluminum-substituted cobalt ferrite films with magneto-optical activity to a silicon microring resonator is suggested. The strong remanent magnetization of the employed magneto-optical material allows the operation of the device without any external magnetizing elements, and the device footprint is only 150 μm^2. A prototype chip has been fabricated using conventional processes compatible with the silicon on an insulator platform, and a maximum isolation ratio of 7 dB at the 1557.6 nm wavelength has been achieved. To the best of our knowledge, this is the most compact photonic isolator demonstrated to date, and it is suitable for all-optical circuits with extremely high integration density.

1. INTRODUCTION

Isolators are nonreciprocal components that provide protection against back-reflected light arising from unmatched loads in photonic integrated circuits (PICs). These parasitic reflections have the potential to disturb the stable operation of signal sources, such as semiconductor lasers, and, in the worst-case scenario, to damage the most sensitive components of the circuit [1–5].

The nonreciprocal features of isolators are often related to the time-reversal symmetry breaking provided by the utilization of magneto-optical (MO) materials in their designs. However, typical MO materials display useful activity only when the magnetization is saturated by external magnets [6–9]. In addition, TE polarized light is often dominant and easier to achieve in conventional semiconductor lasers [10–13], while current integration techniques of MO materials to silicon on insulator (SOI) substrates favor the design of nonreciprocal devices operating with TM modes [14–16].

For example, TM-mode isolators operating at the 1550 nm wavelength are suggested in [17, 18]. These devices consist of a SOI microring resonator (MRR) bonded to a MO layer made of a cerium-substituted yttrium iron garnet (Ce:YIG). The magnetization of the Ce:YIG thin film is saturated by a gold microstrip coil in these components, and their footprints are in the range of a few thousand square micrometers.

A TE-mode optical isolator for operation at the 1550 nm wavelength is proposed in [19]. This device consists of an asymmetric SOI ring resonator onto which a Ce:YIG layer is integrated by a wafer bonding technique. The resonator displays nonreciprocal phase shift (NRPS) for TM modes, and two built-in TE-TM polarization rotators enable the isolation for TE modes. The device operates under an unidirectional magnetic field, and its footprint is estimated to be 130,000 μm^2.

The requirement for external magnets in the isolator designs presented in [17–19] does not favor compactness and introduces packaging issues, since such elements are usually cumbersome. Furthermore, electromagnets present additional challenges for the operation of photonic isolators, such as wavelength detuning caused by Joule heating.

Regarding the isolator designs proposed in [17–19], the need for polarization rotators with a view to their utilization in conjunction with semiconductor lasers supporting TE modes, as well as the lower confinement of TM modes in dielectric waveguides (in comparison to TE modes), also compromises further miniaturization of these devices.

Additionally, the remaining thick (Ca, Mg, Zr)-substituted gadolinium gallium garnet (SGGG) substrates on which Ce:YIG films are grown pose additional challenges in the isolator designs suggested in [17–19]. In the cases presented in [17, 18], additional polishing processes are required in order to thin down the SGGG substrates and to reduce the distance between the MRR and electromagnet structures. On the other hand, the SGGG layer of the isolator presented in [19] is neither thinned nor removed, which hinders further downsizing of the component.

In this paper, we present a novel isolator for operation with TE modes at the 1550 nm wavelength whose footprint is only 150 μm^2, the smallest already reported for a photonic isolator. The proposed device is two to three orders of magnitude smaller than the designs presented in [17–19], and its ultra-compact size is mainly due to the utilization of thin films made of an aluminum-substituted cobalt ferrite with molecular formula $CoAl_{0.57}Fe_{1.43}O_4$ (CAFO), which display high MO activity even without any bias magnets.

* Corresponding author: Gianni Portela (masaki@unicamp.br).

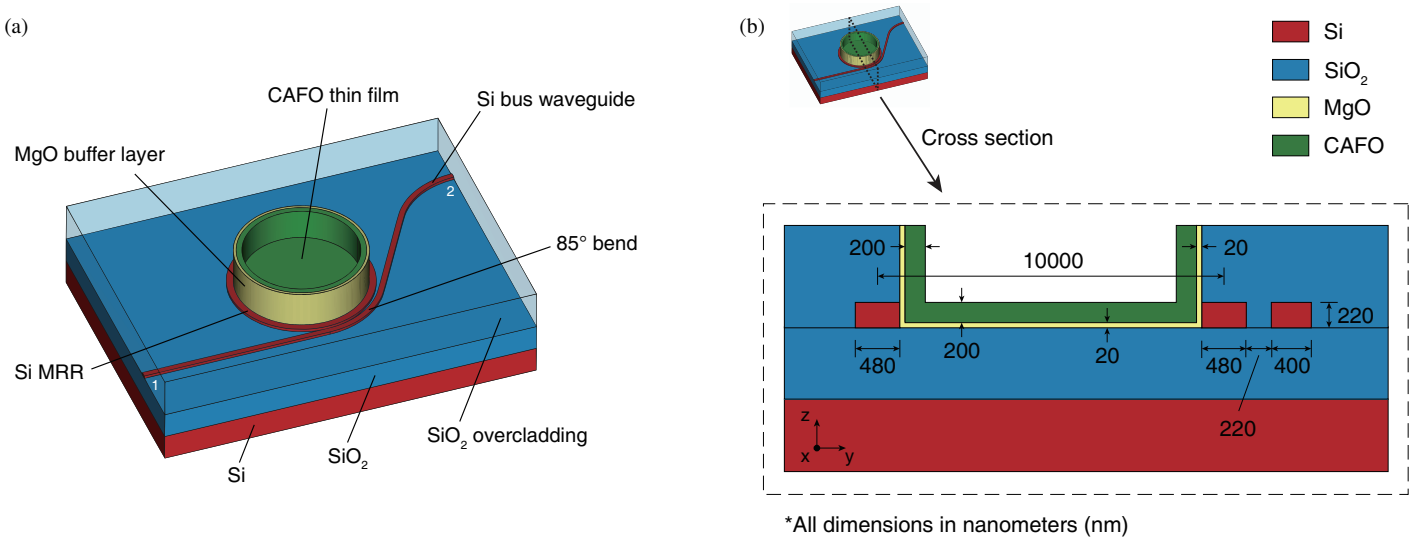

FIGURE 1. Schematic of the bias-free photonic isolator: (a) perspective view and (b) cross-section view.

Despite also employing CAFO thin films as MO media, the TM-mode isolator proposed in [20] has a much larger footprint (3,053 μm^2). Specifically, the lower optical confinement of TM modes requires structures with larger bending radius, and as a consequence, further footprint reduction is very difficult to achieve in this case.

The native operation of the proposed isolator with TE modes (without the need for polarization rotators), as well as the monolithic integration of the MO film to the isolator structure with no remaining thick substrates, also contributed to the small device footprint.

2. ISOLATOR DESIGN AND OPERATING PRINCIPLE

The suggested bias-free photonic isolator is based on a SOI substrate in which an MRR and a bus waveguide are patterned. The entire structure is covered by a silica (SiO_2) overcladding containing a window for the deposition of a 200 nm-thick CAFO film, as schematically shown in Figure 1. The bias-free operation of the device, that is, without any external magnets, is ensured by the strong remanent magnetization of the deposited CAFO thin film. A comprehensive study of the MO properties of CAFO thin films, including measurements of material loss and hysteresis loops, is presented in [20].

The deposition of the CAFO thin film is assisted by a predeposited 20 nm-thick magnesium oxide (MgO) buffer layer. The MgO layer reduces the lattice mismatch between the CAFO film and the Si substrate, and allows the deposition of highly oriented CAFO films with lower losses [20, 21].

The cross-section dimensions of the MRR are 480 nm × 220 nm, while those of the bus waveguide are 400 nm × 220 nm. The radius of the ring resonator is 5 µm, and it supports two counter-rotating TE modes around the 1550 nm wavelength whose degeneracy is removed due to the NRPS effect induced by the deposited CAFO thin film. By operating at one of the MRR resonant wavelengths, isolation for TE modes is attainable.

Temporal coupled-mode theory (TCMT) equations can be used to analyze the device operation. For instance, the TCMT methodology for nonreciprocal devices described in [2] allows one to derive formulas for calculation of the S-parameters $S_{21}(\omega)$ and $S_{12}(\omega)$. A device analysis based on TCMT is presented in Appendix A.

Preliminary computational simulations of the device considering a typical straight bus waveguide demonstrated that the gap (g) between the bus waveguide and MRR should be 15 nm to maximize the isolation ratio (IR) of the proposed design. However, such small gap would not be feasible, considering the limitations on the available fabrication methods.

In order to enable the fabrication of the device and to compensate the lower coupling between the bus waveguide and MRR as a result of a larger gap, a racetrack resonator could be considered, but at the expense of a larger device footprint and narrower free spectral range (FSR). Alternatively, we have designed a waveguide bend with bending angle θ in order to address this issue with no further increase in the device footprint. A parametric optimization has been carried out to define the values of θ and g that would maximize the device IR level, resulting in $\theta = 85°$ and $g = 220$ nm.

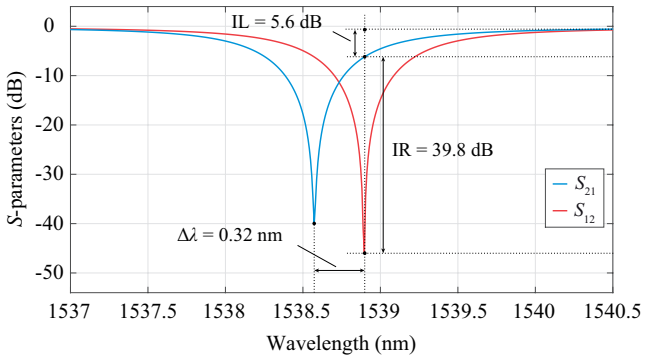

FIGURE 2. S-parameters of the isolator obtained from computational simulations.

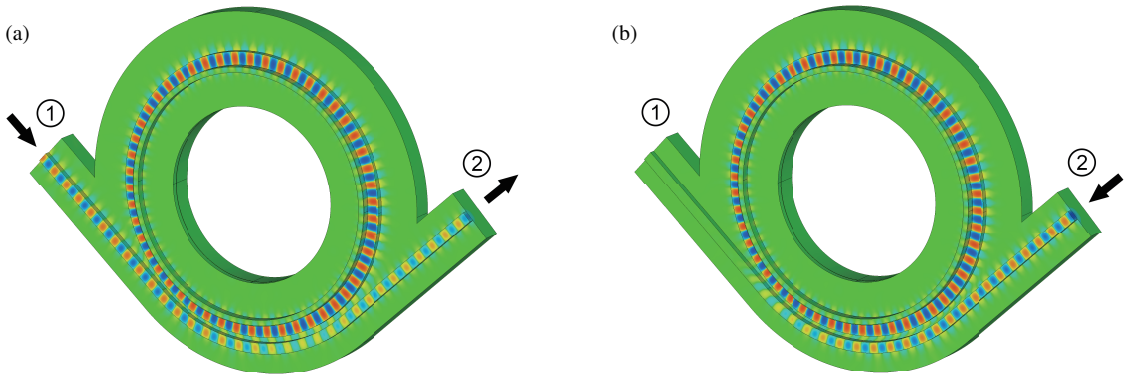

FIGURE 3. H_z distribution at the 1538.9 nm wavelength for input signals applied to (a) port 1 and (b) port 2.

It should be noted that both CAFO and other MO materials, such as Ce:YIG, can induce the NRPS effect required for the operation of MRR-based photonic isolators. However, the attractive features of CAFO thin films, such as their strong remanent magnetization and straightforward integration onto SOI substrates via sputtering techniques, make them more suitable for developing photonic isolators with a smaller footprint, simpler operation, and easier fabrication.

3. COMPUTATIONAL SIMULATIONS

Three-dimensional computational simulations of the isolator design have been performed with the full-wave electromagnetic solver CST Studio Suite, with a view to confirm the device feasibility and to obtain the best design in terms of IR and insertion loss (IL) levels.

We have considered in our computational simulations that the refractive indexes of Si, SiO_2, and MgO are equal to 3.46, 1.45, and 1.72, in that order [22–24]. In addition, the refractive index, extinction coefficient, and Faraday rotation coefficient of the CAFO material in our numerical calculations are equal to 2.4, 0.014, and 22,000 deg/cm, respectively [20, 25].

The calculated S-parameters $S_{21}(\lambda)$ and $S_{12}(\lambda)$ are shown in Figure 2.

At the 1538.9 nm wavelength, the IL and IR levels are 5.6 dB and 39.8 dB, respectively, with a wavelength splitting ($\Delta\lambda$) equal to 0.32 nm. In addition, the calculated FSR of the MRR is approximately 18.5 nm and the device bandwidth around each of the MRR resonant wavelengths, defined at the 10 dB IR level, is 23 GHz.

The H_z component profile at the 1538.9 nm wavelength is presented in Figure 3. One can verify from Figure 3(a) that an input signal applied to port 1 is transmitted to port 2, since the coupling between the input signal and MRR modes is weak in this situation. On the other hand, as illustrated in Figure 3(b), an input signal applied to port 2 is strongly coupled to the clockwise rotating mode of the MRR at this wavelength, resulting in high isolation of port 1. The SiO_2 overcladding is omitted in Figure 3 for better visualization of the field profiles within the component.

4. DEVICE FABRICATION

The fabrication process flow of the isolator is presented in Figure 4. A SOI wafer consisting of Si (220 nm)/SiO_2/Si layers with pre-deposited SiO_2 mask layer was used in the fabrication of the prototype chip.

Firstly, the SOI wafer was coated with ZEP520A electron beam (EB) resist, and an EB lithography (EBL) step has been performed in order to pattern the resist. Subsequently, the SiO_2 mask layer and 220 nm-thick Si layer have been patterned by reactive ion etching (RIE) in CF_4 and SF_6 plasmas, respectively. An HF solution has been used to remove the remaining SiO_2 mask layer and to complete the patterning of the isolator structure.

After that, we have employed plasma-enhanced chemical vapor deposition (PECVD) to deposit a 1 µm-thick SiO_2 cladding over the patterned wafer. A window for the deposition of the CAFO thin film was etched in the overcladding by maskless photolithography (PL) with AZ5218E resist and RIE in CF_4 plasma. Finally, a 20 nm-thick MgO buffer layer and a 200 nm-thick CAFO thin film have been deposited inside the window by RF magnetron sputtering, following the procedures described in [20].

A top view of the fabricated chip obtained by optical microscopy and a perspective view captured using scanning electron microscopy (SEM) are shown in Figures 5 and 6, respectively. These images together provide a clear overview of the key elements of the device.

5. DEVICE CHARACTERIZATION

The transmittance spectrum of the device has been measured by coupling TE-polarized light from lensed fibers into both sides of the Si bus waveguide, in order to measure the device transmittance both in the forward and backward propagation directions. We have adopted an end-fire coupling scheme assisted by an auto-alignment system, and a dicing saw has been used to create the facets for the fiber-chip-fiber coupling [26].

In addition, prior to the transmittance measurements, each of the chip pieces has been magnetized for about 1 minute by an electromagnet producing an out-of-plane magnetic field of 15 kOe, in order to saturate the magnetization of the CAFO thin film. The remanent magnetization of CAFO promotes the

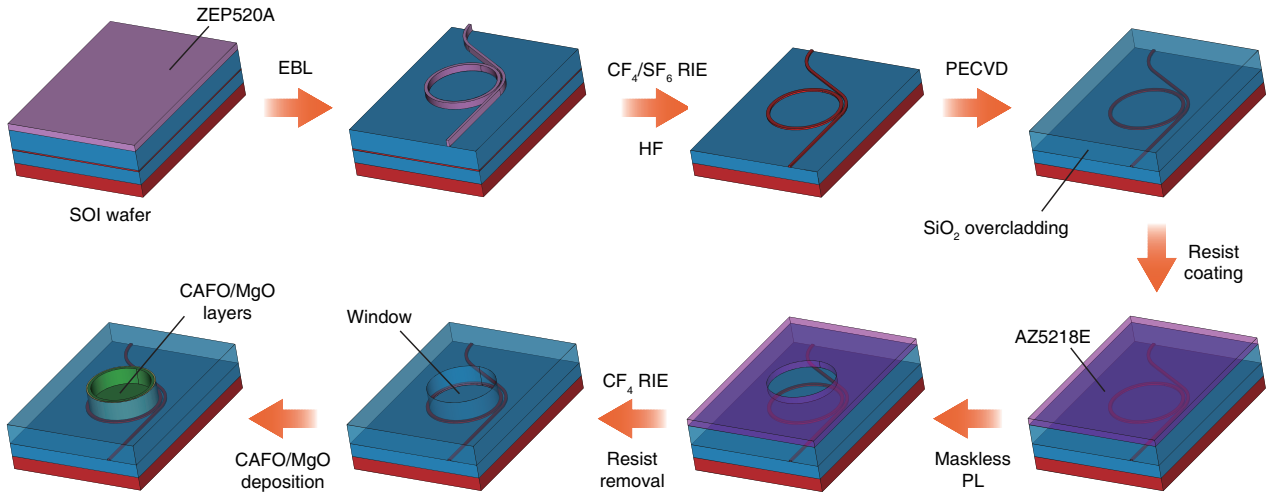

FIGURE 4. Fabrication steps of the bias-free photonic isolator.

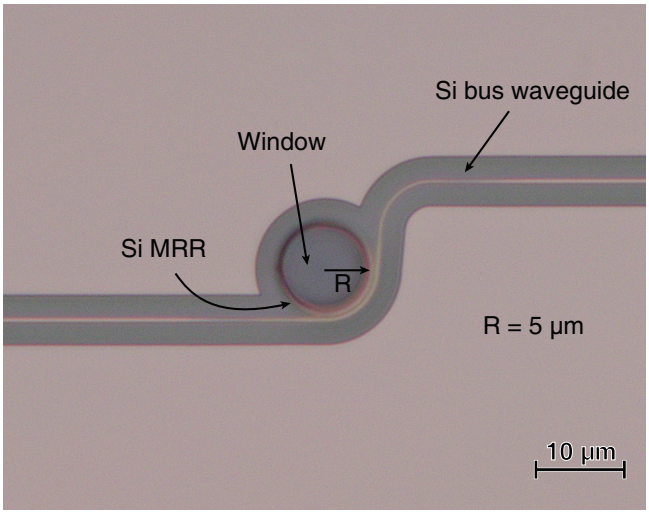

FIGURE 5. Top view of the fabricated chip obtained by optical microscopy (before CAFO deposition).

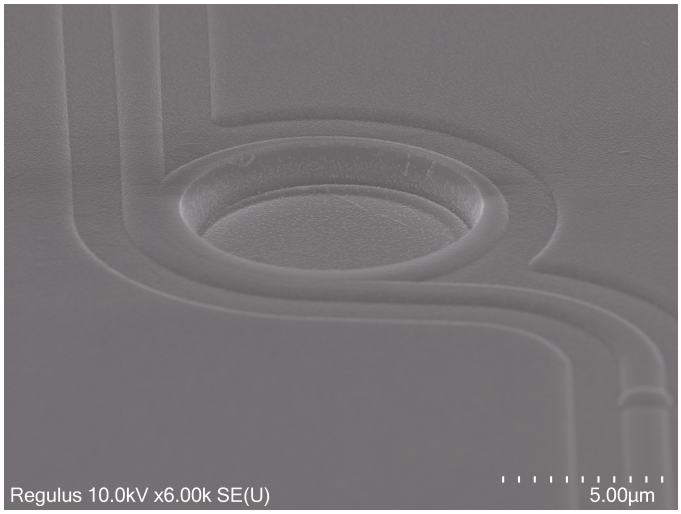

FIGURE 6. SEM perspective view of the fabricated chip.

wavelength splitting between the MRR counter-rotating resonances and ensures the bias-free operation of the device.

The measured transmittance spectrum for TE modes is shown in Figure 7 for both propagation directions. At the 1557.6 nm wavelength, the IL and IR levels are 7.2 dB and 7 dB, respectively. The resonator FSR is approximately 18.2 nm, and the $\Delta\lambda$ parameter is 0.39 nm. One must highlight that the transmittance spectrum presented in Figure 7 corresponds to the sample with the highest IR level among the several samples contained in the prototype chip.

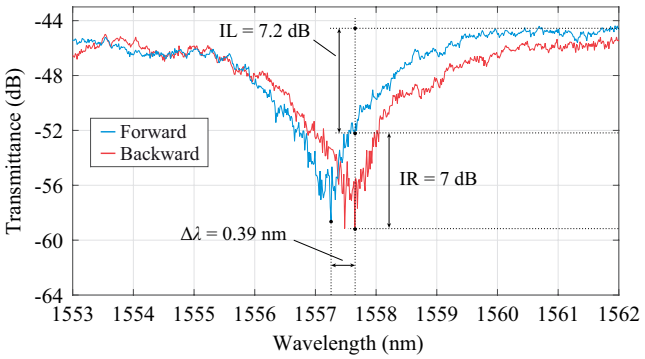

FIGURE 7. Transmittance spectrum of the fabricated isolator.

6. DISCUSSION

The results obtained from computational simulations and experimental measurements are summarized in Table 1 for comparison purposes. Although the simulated and experimental results show good agreement for the $\Delta\lambda$, FSR, and IL parameters, the IR level of the fabricated isolator is significantly lower than the value predicted by device simulations. This difference is likely related to the high absorption losses of the deposited CAFO thin film and to structural imperfections of the fabricated chip.

TABLE 1. Simulated and experimental results.

Data	$\Delta\lambda$ (nm)	FSR (nm)	IL (dB)	IR (dB)
Simulation	0.32	18.5	5.6	39.8
Experimental	0.39	18.2	7.2	7

At the 1550 nm wavelength, the absorption losses of CAFO, of the order of dB/μm [20], are much larger than those of Ce:YIG, which are of the order of dB/cm [17]. In general, the higher the loss is, the higher the overlap is between the resonances of the MO MRR structure and the lower the IR level is.

However, the Faraday rotation coefficient of Ce:YIG is much smaller at the 1550 nm wavelength (about 4,500 deg/cm) [17]. In addition, the thick SGGG substrates on which Ce:YIG thin films are grown occupy a relatively large area and require additional post-bonding fabrication processes, while CAFO thin films can be directly deposited on SOI substrates using buffer layers (e.g., MgO or ZnO) [20], resulting in a smaller device footprint and reducing fabrication complexity. Finally, Ce:YIG films, unlike CAFO films, require external magnets to exhibit significant MO activity.

Therefore, there is a trade-off between using Ce:YIG and using CAFO thin films in the design of nonreciprocal photonic devices. We have chosen CAFO material because it would enable a more compact and easier-to-fabricate isolator design.

As for the isolator fabrication, the alignment of the window etched in the SiO_2 overcladding with the MRR is very challenging, and small deviations can reduce the magnitude of the NRPS effect. In addition, surface roughness of the Si elements causes unwanted scattering of light, resulting in performance degradation [27, 28].

Although it does not achieve an IR level in the range of 20 to 30 dB, as the isolators presented in [17–19] do, the suggested isolator is two to three orders of magnitude more compact. Besides, further improvements in the quality of CAFO thin films through elemental substitution [29] and the use of different buffer layers [30], as well as the optimization of the fabrication process conditions, can potentially enhance device performance.

Some questions not addressed in this paper, such as temperature dependence of CAFO properties and long-term stability of the proposed device, could be explored in future research.

7. CONCLUSION

In summary, a new TE-mode photonic isolator based on the monolithic integration of CAFO thin films to a silicon MRR structure has been demonstrated. By making use of fabrication processes compatible with the SOI platform, we have fabricated a prototype chip with a measured isolation ratio of 7 dB at the 1557.6 nm wavelength.

The bias-free operation of the suggested photonic isolator is made possible by the high remanent magnetization of the deposited CAFO film. The elimination of the bias magnet, the native operation with TE modes (with no need for polarization rotators), and the monolithic integration of the CAFO layer with no remaining substrates enabled a simpler isolator design with reduced footprint.

Compared to conventional isolator designs, in which external magnets are required, the footprint of the proposed photonic isolator (approximately 150 μm^2) is two to three orders of magnitude smaller. As far as we know, this is the most compact isolator demonstrated to date, and large-scale photonic integrated circuits can benefit from it.

ACKNOWLEDGEMENT

This work was partially supported by the Sao Paulo Research Foundation (FAPESP/Brazil) under the projects 2019/13667-0 and 2022/02391-6 (GP's research grants), 2021/11380-5 (CPTEn), 2021/00199-8 (SMARTNESS), and 2022/11596-0 (EMU); and by the National Council for Scientific and Technological Development (CNPq/Brazil), under the project 314539/2023-9 (HEHF's research productivity grant).

The authors would like to thank Professor Miguel Levy from Michigan Technological University (Michigan Tech, USA) for the fruitful discussions on magneto-optical devices.

This work was conducted at Nanofab, Tokyo Tech.

APPENDIX A. TCMT-BASED ANALYSIS OF THE DEVICE

The TCMT methodology presented in [2] can be used to obtain the following formulas for the calculation of the device S-parameters $S_{21}(\omega)$ and $S_{12}(\omega)$:

$$S_{21}(\omega) = 1 - \frac{\gamma_+}{j(\omega-\omega_+)+\gamma_+ + \gamma_{i+}}, \quad \text{(A1)}$$

$$S_{12}(\omega) = 1 - \frac{\gamma_-}{j(\omega-\omega_-)+\gamma_- + \gamma_{i-}}. \quad \text{(A2)}$$

where parameters $\omega_\pm$, $\gamma_\pm$, and $\gamma_{i\pm}$ are the resonant frequency, the decay rate due to waveguide coupling, and the decay rate due to intrinsic losses of the counterclockwise (+) and clockwise (−) MRR rotating modes.

The main benefit of devising a TCMT model of a given device is the possibility of relating the TCMT parameters to the device's geometric/material characteristics. For example, one can derive from (A1) and (A2) that, at $\omega = \omega_-$, S_{12} tends to zero given that $\gamma_- \gg \gamma_{i-}$, while S_{21} tends to one given that $\gamma_+ \gg \gamma_{i+}$ and $|\omega_+ - \omega_-| \gg 0$. In this case, the condition $\gamma_\pm \gg \gamma_{i\pm}$ can be met by tuning the gap between the bus waveguide and the MRR (to increase $\gamma_\pm$) or by using materials with low absorption losses (to decrease $\gamma_{i\pm}$). On the other hand, the utilization of MO materials with high Faraday rotation coefficient is a potential way to ensure that the condition $|\omega_+ - \omega_-| \gg 0$ is satisfied [2]. Similar analysis can be performed considering operation at the resonant frequency ω_+.

In addition, a comparison between the device S-parameters obtained from computational simulations and those obtained from Equations (A1) and (A2) is given in Figure A1.

In Figure A1, we have considered the following values of the TCMT parameters: $\gamma_+ = \gamma_- = 4.5 \times 10^{11}$ rad/s, $\gamma_{i+} = \gamma_{i-} = 2 \times 10^9$ rad/s, $\omega_- = 1.224027 \times 10^{15}$ rad/s, and

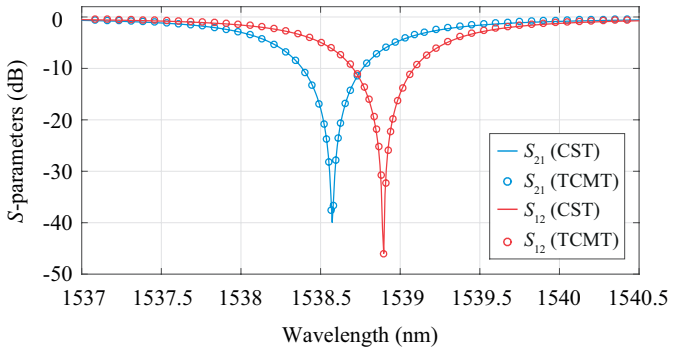

FIGURE A1. S-parameters of the isolator obtained from CST Studio Suite and TCMT formulas.

$\omega_+ = 1.224284 \times 10^{15}$ rad/s. These values have been estimated by manual fitting of the simulation data, and a good agreement between the TCMT and simulation results can be observed. By performing the fitting process, a deeper understanding of how design parameters influence device performance can be acquired.

REFERENCES

[1] Yan, W., Y. Yang, S. Liu, Y. Zhang, S. Xia, T. Kang, W. Yang, J. Qin, L. Deng, and L. Bi, "Waveguide-integrated high-performance magneto-optical isolators and circulators on silicon nitride platforms," *Optica*, Vol. 7, No. 11, 1555–1562, 2020.

[2] Portela, G., M. Levy, and H. E. Hernandez-Figueroa, "Novel compact magnetless isolator based on a magneto-optical garnet material," *Optics & Laser Technology*, Vol. 157, 108638, 2023.

[3] Du, Q., C. Wang, Y. Zhang, Y. Zhang, T. Fakhrul, W. Zhang, C. Gonçalves, C. Blanco, K. Richardson, L. Deng, *et al.*, "Monolithic on-chip magneto-optical isolator with 3 dB insertion loss and 40 dB isolation ratio," *ACS Photonics*, Vol. 5, No. 12, 5010–5016, 2018.

[4] Takeda, H. and S. John, "Compact optical one-way waveguide isolators for photonic-band-gap microchips," *Physical Review A — Atomic, Molecular, and Optical Physics*, Vol. 78, No. 2, 023804, 2008.

[5] Shoji, Y., M. Ito, Y. Shirato, and T. Mizumoto, "MZI optical isolator with Si-wire waveguides by surface-activated direct bonding," *Optics Express*, Vol. 20, No. 16, 18 440–18 448, 2012.

[6] Ghising, P., Z. Hossain, and R. C. Budhani, "Stripe magnetic domains in $CeY_2Fe_5O_{12}$ (Ce:YIG) epitaxial films," *Applied Physics Letters*, Vol. 110, No. 1, 012406, 2017.

[7] Zhang, Y., C. T. Wang, X. Liang, B. Peng, H. P. Lu, P. H. Zhou, L. Zhang, J. X. Xie, L. J. Deng, M. Zahradnik, *et al.*, "Enhanced magneto-optical effect in $Y_{1.5}Ce_{1.5}Fe_5O_{12}$ thin films deposited on silicon by pulsed laser deposition," *Journal of Alloys and Compounds*, Vol. 703, 591–599, 2017.

[8] Miyashita, H., Y. Yoshihara, K. Mori, T. Koguchi, P. B. Lim, M. Inoue, K. Ishiyama, and T. Goto, "Vacuum laser annealing of magnetooptical cerium-substituted yttrium iron garnet films," *Optical Materials*, Vol. 146, 114530, 2023.

[9] Srinivasan, K. and B. J. H. Stadler, "Magneto-optical materials and designs for integrated TE-and TM-mode planar waveguide isolators: A review," *Optical Materials Express*, Vol. 8, No. 11, 3307–3318, 2018.

[10] Zhu, H., S. C. Su, S. F. Yu, W. F. Zhang, C. C. Ling, and H. Y. Yang, "Ultraviolet lasing characteristics of ZnS microbelt lasers," *IEEE Journal of Selected Topics in Quantum Electronics*, Vol. 19, No. 4, 1501705, 2013.

[11] Li, K. H., Y. F. Cheung, W. Y. Fu, and H. W. Choi, "Electrically injected whispering-gallery mode InGaN/GaN microdisks," *Applied Physics Letters*, Vol. 119, No. 10, 101106, 2021.

[12] Heil, T., A. Uchida, P. Davis, and T. Aida, "TE-TM dynamics in a semiconductor laser subject to polarization-rotated optical feedback," *Physical Review A*, Vol. 68, No. 3, 033811, 2003.

[13] Shibasaki, N., A. Uchida, S. Yoshimori, and P. Davis, "Characteristics of chaos synchronization in semiconductor lasers subject to polarization-rotated optical feedback," *IEEE Journal of Quantum Electronics*, Vol. 42, No. 3, 342–350, 2006.

[14] Ghosh, S., S. Keyvavinia, W. V. Roy, T. Mizumoto, G. Roelkens, and R. Baets, "Ce:YIG/Silicon-on-Insulator waveguide optical isolator realized by adhesive bonding," *Optics Express*, Vol. 20, No. 2, 1839–1848, 2012.

[15] Chen, W.-T., L. Liu, J. Zhao, and C. Zhang, "On-chip broadband, compact TM mode Mach-Zehnder optical isolator based on InP-on-insulator platforms," *Nanomaterials*, Vol. 14, No. 8, 709, 2024.

[16] Shoji, Y. and T. Mizumoto, "Silicon waveguide optical isolator with directly bonded magneto-optical garnet," *Applied Sciences*, Vol. 9, No. 3, 609, 2019.

[17] Pintus, P., D. Huang, C. Zhang, Y. Shoji, T. Mizumoto, and J. E. Bowers, "Microring-based optical isolator and circulator with integrated electromagnet for silicon photonics," *Journal of Lightwave Technology*, Vol. 35, No. 8, 1429–1437, 2017.

[18] Huang, D., P. Pintus, C. Zhang, Y. Shoji, T. Mizumoto, and J. E. Bowers, "Electrically driven and thermally tunable integrated optical isolators for silicon photonics," *IEEE Journal of Selected Topics in Quantum Electronics*, Vol. 22, No. 6, 271–278, 2016.

[19] Liu, S., Y. Shoji, and T. Mizumoto, "TE-mode magneto-optical isolator based on an asymmetric microring resonator under a unidirectional magnetic field," *Optics Express*, Vol. 30, No. 6, 9934–9943, 2022.

[20] Sato, K., M. Okano, and Y. Shoji, "Ultra-compact microring optical isolator using an aluminum-substituted cobalt ferrite thin film," *Optica*, Vol. 11, No. 6, 889–895, 2024.

[21] Serrano-Núñez, M. A., Y. Shoji, and T. Mizumoto, "Small magnetless integrated optical isolator using a magnetized cobalt ferrite film," *IEICE Electronics Express*, Vol. 19, No. 2, 20 210 500–20 210 500, 2022.

[22] Gao, L., F. Lemarchand, and M. Lequime, "Exploitation of multiple incidences spectrometric measurements for thin film reverse engineering," *Optics Express*, Vol. 20, No. 14, 15 734–15 751, 2012.

[23] Nejadmalayeri, A. H., P. R. Herman, J. Burghoff, M. Will, S. Nolte, and A. Tünnermann, "Inscription of optical waveguides in crystalline silicon by mid-infrared femtosecond laser pulses," *Optics Letters*, Vol. 30, No. 9, 964–966, 2005.

[24] Serrano-Núñez, M. A., Y. Shoji, and T. Mizumoto, "Design of ultra-compact TE mode ring optical isolator using a cobalt ferrite film for silicon photonic integrated circuits," *Japanese Journal of Applied Physics*, Vol. 60, No. 9, 092003, 2021.

[25] Suzuki, K., T. Namikawa, and Y. Yamazaki, "Preparation of zinc- and aluminum-substituted cobalt-ferrite thin films and their Faraday rotation," *Japanese Journal of Applied Physics*, Vol. 27, No. 3R, 361, 1988.

[26] Ishida, E., K. Miura, Y. Shoji, H. Yokoi, T. Mizumoto, N. Nishiyama, and S. Arai, "Amorphous-Si waveguide on a garnet magneto-optical isolator with a TE mode nonreciprocal phase

shift," *Optics Express*, Vol. 25, No. 1, 452–462, 2017.

[27] Grillot, F., L. Vivien, S. Laval, D. Pascal, and E. Cassan, "Size influence on the propagation loss induced by sidewall roughness in ultrasmall SOI waveguides," *IEEE Photonics Technology Letters*, Vol. 16, No. 7, 1661–1663, 2004.

[28] Bellegarde, C., E. Pargon, C. Sciancalepore, C. Petit-Etienne, V. Hugues, D. Robin-Brosse, J.-M. Hartmann, and P. Lyan, "Improvement of sidewall roughness of submicron SOI waveguides by hydrogen plasma and annealing," *IEEE Photonics Technology Letters*, Vol. 30, No. 7, 591–594, 2018.

[29] Martens, J. W. D., W. L. Peeters, P. Q. J. Nederpel, and M. Erman, "The polar magneto-optical Kerr effect and the dielectric tensor elements of $CoFe_{2-x}Al_xO_4$ $0.1 \leq x \leq 1$ in the photon energy range $0.65 \leq h\nu \leq 4.5$ eV," *Journal of Applied Physics*, Vol. 55, No. 4, 1100–1104, 1984.

[30] Ortiz, G., A. García-García, N. Biziere, F. Boust, J. F. Bobo, and E. Snoeck, "Growth, structural, and magnetic characterization of epitaxial Co_2MnSi films deposited on MgO and Cr seed layers," *Journal of Applied Physics*, Vol. 113, No. 4, 043921, 2013.